

Green Chemistry

Cutting-edge research for a greener sustainable future

Accepted Manuscript

View Article Online
View Journal

This article can be cited before page numbers have been issued, to do this please use: N. Guenani, J. Solera Rojas, D. Carvajal, C. Mejuto, A. Mollar-Cuni, A. Guerrero, F. Fabregat-Santiago, J. A. Mata and E. Mas-Marzá, *Green Chem.*, 2024, DOI: 10.1039/D4GC01275E.



This is an Accepted Manuscript, which has been through the Royal Society of Chemistry peer review process and has been accepted for publication.

Accepted Manuscripts are published online shortly after acceptance, before technical editing, formatting and proof reading. Using this free service, authors can make their results available to the community, in citable form, before we publish the edited article. We will replace this Accepted Manuscript with the edited and formatted Advance Article as soon as it is available.

You can find more information about Accepted Manuscripts in the [Information for Authors](#).

Please note that technical editing may introduce minor changes to the text and/or graphics, which may alter content. The journal's standard [Terms & Conditions](#) and the [Ethical guidelines](#) still apply. In no event shall the Royal Society of Chemistry be held responsible for any errors or omissions in this Accepted Manuscript or any consequences arising from the use of any information it contains.

Data availability statements

The data supporting this article have been included as part of the Supplementary Information

Room temperature hydrogen production via electro-dehydrogenation of amines into nitriles: advancements in Liquid Organic Hydrogen Carriers

Nihal Guenani,¹ Jose Solera-Rojas,¹ David Carvajal,¹ Carmen Mejuto,¹ Andrés Mollar-Cuni,¹ Antonio Guerrero,¹ Francisco Fabregat-Santiago,¹ José A. Mata,^{*1} and Elena Mas-Marzá^{*1}

¹ Institute of Advanced Materials (INAM), Universitat Jaume I, 12006 Castelló, Spain.

Email: jmata@uji.es and emas@uji.es

Abstract

This study introduces an electro-dehydrogenation method for converting amines into nitriles in aqueous environments, simultaneously releasing two moles of H₂ using nickel electrodes. This eco-friendly process is selective and operates at room temperature, in contrast to traditional thermal methods that require high temperatures and where condensation products are usually observed. Detailed impedance spectroscopy analysis reveals that the dehydrogenation of amines in aqueous media is facilitated by efficient charge transfer, with the diffusion of amines to the electrode surface identified as the kinetically slowest step. Our study underscores the potential of electrochemistry to enhance the reversible dehydrogenation and hydrogenation of the amine/nitrile pair. By demonstrating the practicality and efficiency of this approach, we highlight the amine/nitrile pair as a promising candidate for Liquid Organic Hydrogen Carriers. This has significant implications for the future of hydrogen storage and transport technologies, paving the way for more sustainable and efficient energy solutions.

Keywords: hydrogen production, hydrogen storage, LOHCs, electrocatalysis, nickel electrodes, primary amine electro-dehydrogenation



Introduction

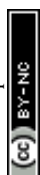
View Article Online
DOI: 10.1039/D4GC01275E

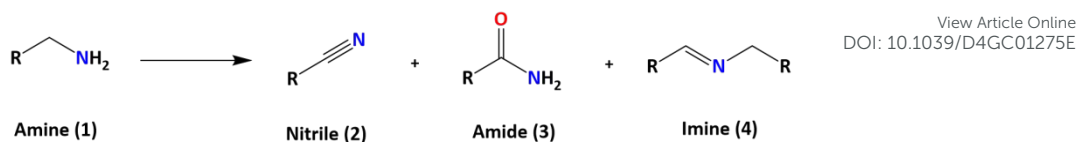
The global climate crisis has intensified the need to adopt renewable energy sources to reduce greenhouse gas emissions and mitigate climate change. Recent energy transition plans, adopted by most countries, emphasize the importance of integrating renewable energies into large-scale industrial applications. However, one of the most significant challenges associated with renewable energy sources is their intermittent nature, which poses issues of stability and reliability in energy supply.¹

Hydrogen has emerged as a promising energy vector due to its favorable properties, including high energy density and the potential to generate energy without pollutant emissions. However, the storage and transportation of hydrogen present considerable challenges. In this context, Liquid Organic Hydrogen Carriers (LOHCs) emerge as a viable solution for storing hydrogen safely, efficiently, and non-toxically. LOHCs enable the chemical storage of hydrogen in liquid organic compounds, facilitating its handling and large-scale transportation.^{2–5}

Water electrolysis is a well-established technology for producing pure hydrogen safely and cleanly, through hydrogen evolution reactions (HER) and oxygen evolution reactions (OER). However, the oxygen evolution reaction, stemming from water splitting, is kinetically and thermodynamically unfavorable, limiting the overall efficiency of the process.⁶ To improve the energy balance of the reaction, a promising strategy is to replace oxygen evolution with the oxidation of less energy-intensive organic substrates, obtaining value-added products in the same process.^{7,8}

Among the systems susceptible to replace OER, oxidation of primary amines represents an attractive option. The oxidation of amines can produce various species, such as aldehydes, ketones, imines, and nitriles (Scheme 1). Specifically, the selective oxidation of primary amines to nitriles is of great interest due to the importance of nitriles as intermediates in chemical synthesis.^{9–14} Additionally, this process can be energy-efficient and operable at low temperatures through electrocatalytic processes.





Scheme 1. Possible products for the dehydrogenation of amines

Different and prestigious research groups in the field of electrochemistry have reported the dehydrogenation of amines using Nickel as electrocatalyst. For example, Z. Bin et al., have described the use of NiSe nanorods as electrodes for the oxidation of aromatic and aliphatic primary amines in basic media.¹⁵ However, this electrocatalyst requires a complex synthetic process, hindering its scalability for industrial use. Similarly, Z. Yan, in collaboration with the research group of Z. Xu, recently reported a hybrid water electrolyzer based on a Ni/Co metal-organic framework for the oxidation of aromatic and aliphatic amines, but only with a single amine functional group in the system.¹⁶ More recently, Choi K-S. has reported the electro-oxidation behavior of propylamine and benzylamine using NiOOH electrodes onto fluorine-doped tin oxide (FTO), analyzing in detail the effect of different parameters in the reaction, such as the amine concentration and pH solution among other factors.¹⁷

Despite advances in amine oxidation, most catalysts developed so far require complex synthetic processes and high temperatures, making scalability for industrial applications challenging. In this work, we propose the use of nickel foam electrodes decorated with Ni (NiNF) as catalysts for the oxidation of primary amines to nitriles in aqueous media without additives, producing molecular hydrogen as the only byproduct. Detailed impedance spectroscopy analysis reveals mechanisms insight related to the response of our nickel electrode. Building on the significant catalytic performance observed in the electrochemical dehydrogenation of amines to nitriles, as well as the hydrogen storage capacity (HSC)¹⁸ of the pair amine/nitriles, we investigated the reverse process: the thermocatalytic hydrogenation of nitriles using molecular H₂ as the hydrogen source. This study demonstrates the potential of the amine/nitrile pair as liquid organic hydrogen carriers (LOHCs).



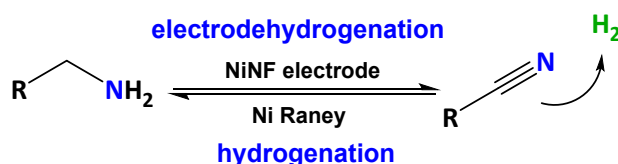


Figure 1. Electro-dehydrogenation/hydrogenation cycle for the use of pair amine/nitrile as LOHCs.

Results and discussion

Our initial focus involved examining the catalytic dehydrogenation of amines to nitriles through electrochemical methods (electro-dehydrogenation) in aqueous basic media at ambient temperature. Various nickel-based electrodes were tested as anodes, leveraging the exceptional electrochemical oxidation performance of nickel for organic molecules under alkaline conditions.¹⁴⁻¹⁶ The Ni-based electrodes employed in this work include Ni foil, Ni foam (NF), Ni foam decorated with nickel (NiNF), Pencil Graphite Rods decorated with Ni (NiPGR) and Ni45, prepared by powder metallurgy following a previous procedure developed in our research group.¹⁸ The deposition of nickel on PGR and Ni foam was performed by electrodeposition. Details for the preparation of the electrodes are described in the supporting information, including microscopy characterization (see section S1.2).

Prior to use, all the electrodes were activated via cyclic voltammetry (CV), in 1 M KOH, to increase the amount of Ni^{3+} active species at the surface of the electrode (see Supporting Information Figure S2). The reversible redox peak observed during the activation corresponds to the transformation of $\alpha/\beta\text{-Ni(OH)}_2$ (Ni^{2+}) to catalytically active $\gamma/\beta\text{-NiOOH}$ (Ni^{3+}), reported in previous studies.¹⁹ The current density associated with the $\text{Ni}^{2+}/\text{Ni}^{3+}$ peak increases for each cycle as a result of increasing the concentration of active species on the electrode surface.

Figure 2a depicts the response of all electrodes in 1 M KOH after activation. As anticipated, NiPGR and NiNF demonstrate elevated current densities at the $\text{Ni}^{2+}/\text{Ni}^{3+}$ redox peak, attributed to a higher concentration of nickel active species on their surfaces compared to Ni foil, NF, and Ni45. The comparison of cyclic voltammogram curves between NF and NiNF emphasizes a notable increase in current density resulting from the incorporation of nickel species through electrodeposition on Ni foam (Figure 2b).



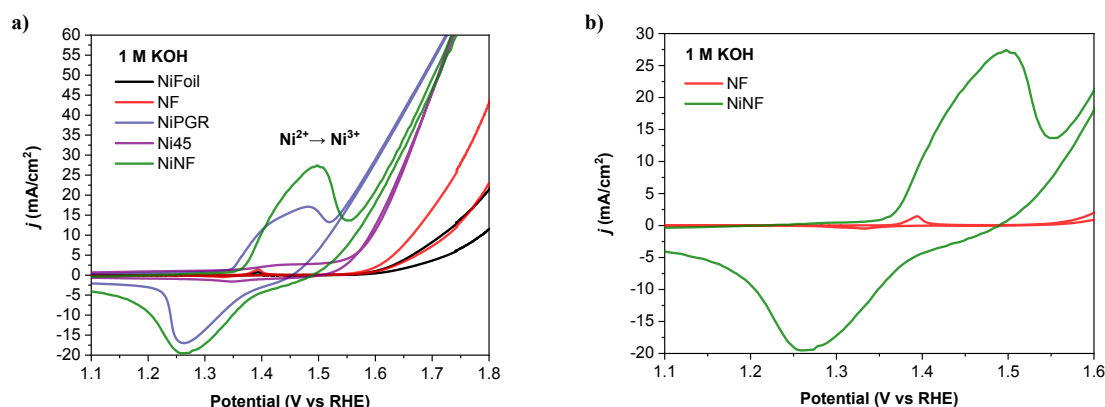


Figure 2. a) Cyclic voltammetries curves at a scan rate of $10 \text{ mV} \cdot \text{s}^{-1}$ of all Ni electrodes in 20 mL of 1 M KOH. b) Detail of a) for a better comparison of NF and NiNF cyclic voltammetries

The electrocatalytic activity of Ni electrodes was assessed in dehydrogenation (oxidation) of amines using 1,6-hexanediamine (**1a**) as model substrate. The use of this compound is convenient for hydrogen storage purposes as it contains two amino functional groups ($-\text{CH}_2\text{-NH}_2$) capable of generating two nitrile groups ($-\text{CN}$), with the concomitant formation of 4 moles of hydrogen, representing a hydrogen storage capacity (HSC) value of 6.9 wt % of hydrogen.

To get a first insight on how the electrodes operate in the presence and absence of **1a**, we first analyzed the cyclic voltammetry (CVs) of the different electrodes under study. Figure 3 shows a representative example using a NiNF electrode in the presence and absence of 25 mM of **1a**. As can be seen, these CVs are very different and there is a noticeable shift in the onset of the $\text{Ni}^{2+}/\text{Ni}^{3+}$ peak towards a higher potential in the presence of **1a**, that may be attributed to the amount of diamine adsorbed onto the electrode surface. Due to the overlap between the oxidation of the diamine **1a** and the oxidation of Ni^{2+} to Ni^{3+} , the peak extends over a longer voltage range. Additionally, there is an increase in the current density which is very clear in the range between 1.5 V and 1.7 V. Besides, the positive current obtained at these potentials in the reverse direction indicates the irreversible oxidation of **1a**, which also consumes some Ni^{3+} species yielding to the smaller reduction peak observed for Ni.



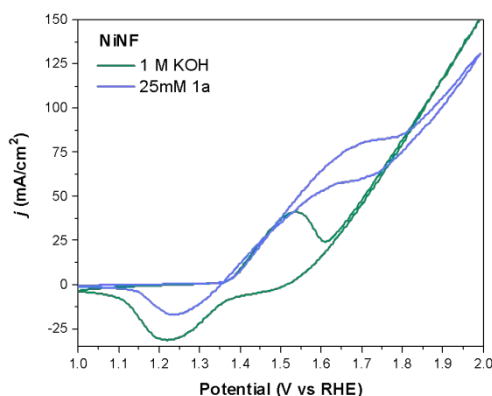


Figure 3. Comparison of cyclic voltammetry curves of NiNF, in 20 mL of 1 M KOH, with and without **1a**.

Then, we explored the performance of our different Ni electrodes in the electrochemical dehydrogenation of **1a** through chronocoulometric experiments. This process involves applying the theoretical charge needed to convert completely **1a** into **2a** at 1.55 V vs RHE, considering a total of eight electrons involved in the process (SI for details). The experimental set-up consists of a two-compartment cell, utilizing a Nafion 117 membrane to prevent potential reduction of oxidation products by the counter electrode (Figure 4). Both the cathodic and anodic chambers were filled with a water solution of KOH as electrolyte, and the required amount of **1a** was introduced in the anodic chamber, under magnetic stirring. The Ni electrodes, with an active area of 2 cm², were immersed in the cell for the duration of the experiments. A platinum electrode was used as a cathode.

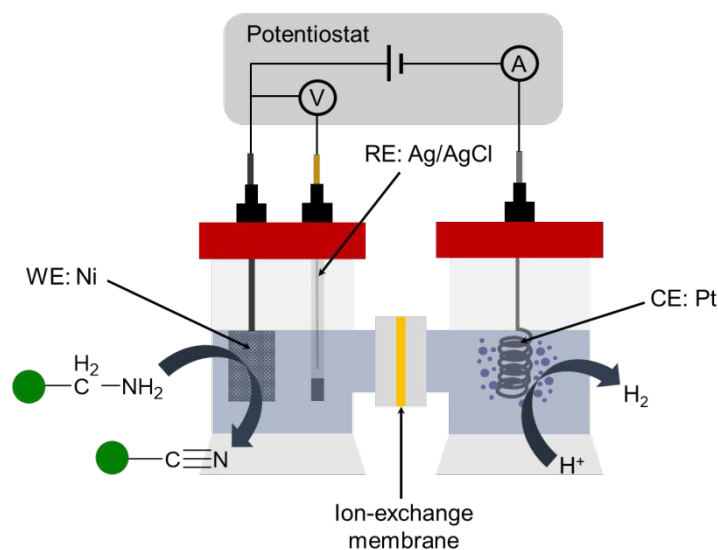


Figure 4. Scheme of two-compartment cell.

The performance of our Ni-based electrodes in the chronocoulometric dehydrogenation of **1a** is shown in Table 1 at room temperature. The total charge passed during the process was 392 C, corresponding to the theoretical charge required for the oxidation of **1a** into **2a**. Detection and quantification of reactants and products were carried out through ¹H-NMR spectroscopy, with ethylene glycol (EG) serving as an internal integration standard. A common problem found in amine dehydrogenation is selectivity. In fact, under thermal catalytic conditions, the formation of condensation products (imines and related products) is generally observed^{20,21} and only a few ruthenium homogeneous catalysts induce complete selectivity towards the formation of nitriles.^{22,23} The electro-dehydrogenation of 1,6-hexanediamine (**1a**) proceeds through the intermediates 1-amino-5-cyanopentane (**i**) and 1-amino-6-imino-hexane (**ii**) (Figure 5). However, these intermediates have not been observed during our experiments due to their high reactivity in comparison to the parent diamine (**1a**).

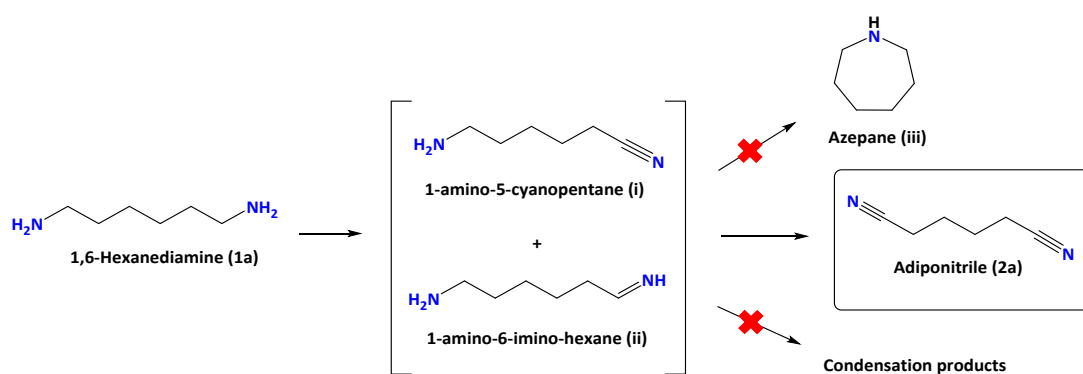
**Figure 5.** Selective electro-oxidation of **1a** targeted in this work.

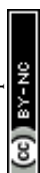
Table 1. Performance of Ni-based electrodes in electro-dehydrogenation of 1a .						
Entry	Electrode	<i>J</i> (mA/cm ²)	<i>t</i> (h)	FE (%)	Conver. (%)	Yield (%)
1	Ni foil	8	150	0	0	0
2	NF	20	20	59	90	60
3	NiPGR	15	12	51	99	52
4	Ni45	55	6	36	94	37
5	NiNF	77	3.5	77	99	78



Reaction conditions: 1,6-hexanediamine (**1a**) (0.5 mmol, 25 mM), 1 M KOH (20 mL), 25 °C at 1.55 V vs RHE. Conversions and yields were determined by ¹H-NMR spectroscopic analysis using ethylene glycol as an external standard. *J* represents the current density at the beginning of the chronocoulometry experiment.

The dehydrogenation of **1a** did not occur with Ni foil as electrode even after 150 hours of reaction, most likely due to the limited active area of this electrode in comparison to the other nickel catalysts (Entry 1, Table 1). All the charge in this experiment was consumed in the competing oxygen evolution reaction (OER). A notable enhancement in electro-dehydrogenation of **1a** was evident when using the other electrodes, particularly those containing electrodeposited nickel. In Entry 5, it is demonstrated that the NiNF electrode exhibited the shortest time to complete conversion of **1a** (~ 3.5 hours), with the highest faradaic efficiency (FE) and yield for the target product **2a**. Conversely, NF, NiPGR, and Ni45, displayed high conversions but suffered yield losses. This discrepancy between conversion and yield stemmed from the instability of **2a** in strong basic media (Figure S16-17). Interestingly, reducing the KOH concentration from 1 M to 0.5 M enabled nearly quantitative yield for **2a**, suggesting the prevention of degradation into undesired species under these conditions (Table 2). However, further reduction in KOH concentration to 0.25 M did not improve the reaction performance, as the current density sharply decreased, and the oxidation reaction time increased significantly (Entry 3, Table 2). This decline in reaction performance might be attributed to a less efficient generation of the Ni redox pair required for the electrochemical oxidation of **1a** when utilizing only 0.25 M of KOH, aligning with our previous investigations on the oxidation of organic compounds with Ni-based electrodes.²⁴ Interestingly, in all our chronocoulometric experiments we have observed that electro-dehydrogenation of **1a** is completely selective to the formation of the corresponding adiponitrile (**2a**) avoiding the formation of undesired intermediates such as cyclization species or condensation products. This observation highlights that the electro-dehydrogenation of amines by nickel species is 100% selective towards the formation of nitriles.

When the reaction of **1a** was performed in a one-compartment configuration, we obtained a 93% yield and FE for **2a**, with 94% conversion of **1a**, suggesting that there is no significant difference between using a two or one compartment cell for the electrooxidation of **1a**. There are studies that utilize membrane-free setups, as previously



reported for the electrooxidation of benzylamine¹⁶; however, to avoid possible nitrile reduction, we conducted all our experiments using a two-compartment cell.

Table 2. Electrolyte influence in electro-dehydrogenation of **1a**.

Entry	Electrolyte	<i>J</i> (mA/cm ²)	<i>t</i> (h)	FE (%)	Conver. (%)	Yield (%)
1	1 M KOH	77	3.5	77	99	78
2	0.5 M KOH	77	3.25	95	99	96
3	0.25 M KOH	20	24	59	99	60

Reaction conditions: 1,6-hexanediamine (**1a**) (0.5 mmol, 25 mM), 0.25-1 M KOH (20 mL), 25 °C at 1.55V vs RHE. Conversions and yields were determined by ¹H-NMR spectroscopic analysis using ethylene glycol (EG) as an external standard. *J* represents the current density at the beginning of the chronocoulometry experiment.

We assessed the influence of temperature in oxidation of **1a** using NiNF as working electrode and 0.5 M KOH as electrolyte. The oxidation of **1a** proceeds similarly to at room temperature or 40 °C providing quantitative yields and FE. However, when the reaction temperature was increased to 60 °C, although complete conversion was observed, only low yields or FE were observed (Table S1). The low yield and FE at high temperatures has been attributed to degradation (predominantly hydrolysis) of the nitriles at basic pH and high temperatures conditions, as noted from NMR studies. Higher temperatures promote side reactions and decomposition of intermediate species, which in turn reduces the selectivity towards the desired product.

The formation of H₂ during the dehydrogenation of **1a** was confirmed by gas chromatography (Figures S18 and S19). When the reaction was performed in the absence of amine, as expected, H₂ and only traces O₂ gas were detected due to OER, confirming that this process is competing with amine dehydrogenation. However, in the presence of amine, H₂ gas was detected in qualitatively amounts and the intensity increased in comparison when performing the reaction without amine. These results suggest that in the presence of **1a**, the OER is suppressed and all the increase in intensity of the signal corresponding to the H₂ gas formed proceeds from the -CH₂NH₂ group of the amine.



To investigate the stability of NiNF, we conducted a series of chronocoulometry experiments using the same electrode five times for the electrooxidation of 25 mM **1a** in 0.5 M KOH observing no significant losses in FE and yield for the formation **2a** (Table S2); thus, demonstrating high stability of our NiNF.

Reaction scope.

Once we establish the optimal reaction conditions for the electrochemical dehydrogenation of **1a**, the efficiency of NiNF electrodes was tested with different primary amines (Table 3). The results showed good versatility with various substrates, including aromatic and aliphatic amines.

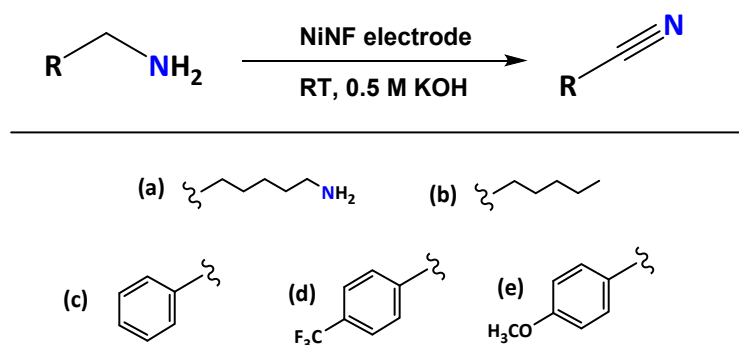


Table 3. Electro-dehydrogenation of primary amines using NiNF electrodes

Entry	Substrate	FE (%)	Yield (%)
1	(a) 1,6-hexanediamine	95	96
2	(b) n-hexylamine	89	90
3	(c) benzylamine	75	77
4	(d) <i>p</i> -trifluoromethylbenzylamine	80	80
5	(e) <i>p</i> -methoxybenzylamine	99	98

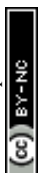


Reaction conditions: amine (**a-e**) (0.5 mmol, 25 mM), 0.5 M KOH (20 mL), 25 °C at 1.55V vs RHE, NiNF electrode. Yields of nitrile were determined by ¹H-NMR spectroscopic analysis using ethylene glycol (EG) as an external standard.

Importantly, all substrates were selectively converted to the corresponding nitrile derivatives in almost quantitative yields. Substrates **1a** and **1b** exhibit similar yields, suggesting that in the case of the diamine, both functional groups operate completely independently despite belonging to the same molecule. Regarding the aromatic substrates, a slight effect is observed depending on the substituent groups at the *para*-position of the aromatic rings, with an increase in the yield value as the nucleophilic substituent strengthens (Entry 3-5, Table 3). The best results were obtained with 1,6-hexanediamine (**1a**) and *p*-methoxybenzylamine (**1e**) which provided yields of 96% and 98%, respectively and high faradaic efficiencies (95% and 99%, respectively).

Detailed electrochemical analysis

The cyclic voltammetry profile of the electrode closely resembled prior investigations involving nickel oxo-hydroxo (NiOOH) electrodes employed for the oxidation of organic substrates.²⁵ For the sample without amine, the redox peak is attributed to the Ni⁺²/Ni⁺³ redox process.¹⁹ In the presence of **1a**, the oxidation current displaces the oxidation peak and the baseline upwards. At the same time the reduction peak decreases indicating that part of the Ni⁺³ has been already reduced during the reduction cycle of the voltammetry of Nickel. The current density (*J*) achieved at the redox peaks associated to the oxidation of Ni and **1a** increased with the concentration of the amine, until reaching a value of ~ 80 a) mA/cm² in the forward direction (~ 60 mA/cm² in the reverse direction) at a 25 mM concentration of **1a**.



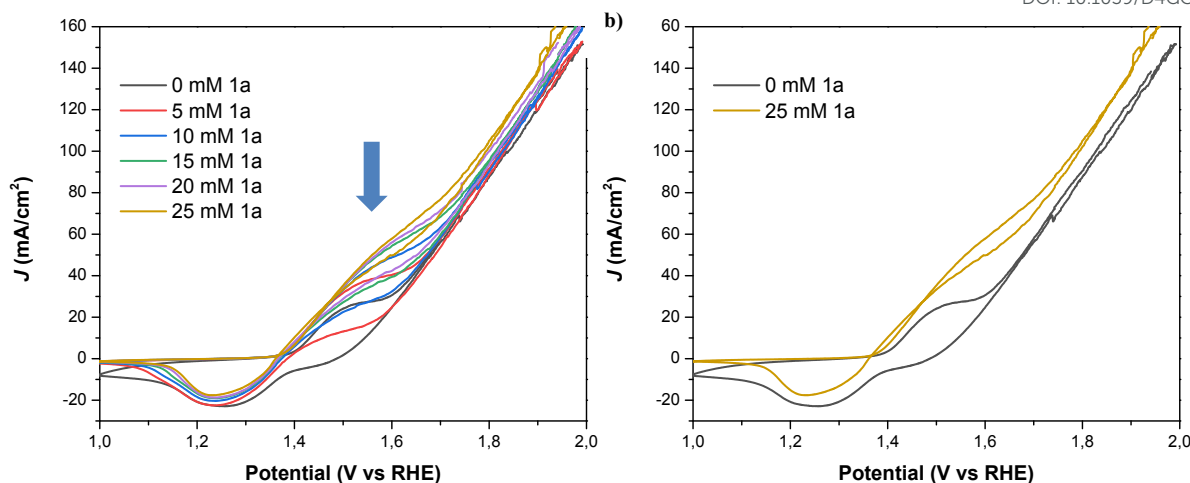


Figure 6. a) Cyclic voltammeteries for the oxidation of **1a** (0-25 mM), using NiNF as working electrode, Pt wire as counter electrode and Ag/AgCl as reference (RHE potential scale), in 0.5 M KOH as electrolyte at 5 mV/s scan b) zoom cyclic voltammeteries for the oxidation of **1a** (0 and 25 mM)

As can be seen in Figure 6, Ni is initially oxidized from $\text{Ni}(\text{OH})_2$ (Ni^{2+}) to NiOOH (Ni^{3+}), being this later species the oxidizing agent responsible for the amine oxidation. As previously reported, the amine oxidation mechanism involves a rate-limiting hydrogen transfer step where a hydrogen radical from the α -C of the amine is transferred to the NiOOH , leading to the reduction of NiOOH to $\text{Ni}(\text{OH})_2$ and amine oxidation.¹⁷ The second oxidation peak observed in the CV, which is overlapped with the $\text{Ni}(\text{OH})_2/\text{NiOOH}$ redox couple, is associated with amine oxidation. This second peak increases with higher amine concentrations. Additionally, the onset and both oxidation peaks ($\text{Ni}^{2+}/\text{Ni}^{3+}$ and amine/nitrile) shift towards higher potentials with increasing amine concentration. This shift is likely due to more amine adsorbed on the electrode, which partially blocks the Ni surface and causes an additional potential loss for Ni oxidation, shifting the amine oxidation reaction by several tens of millivolts.²⁴ If we focus now on the reduction direction of the CV, the reduction peak at 1.3-1.4 V for the $\text{Ni}^{3+}/\text{Ni}^{2+}$ redox couple, decreases with increasing amine concentration. At 1.5 V in the reduction direction, the current remains positive in the presence of amine, indicating ongoing amine oxidation. As Ni^{3+} (or NiOOH) is consumed during this reaction, the height of the Ni^{3+} reduction peak at 1.3-1.4 V diminishes with higher amine concentrations.²⁴



To further examine the performance of NiNF in the electrochemical dehydrogenation of amines, we conducted Current density vs Voltage (J - V) and Impedance Spectroscopy (IS) studies. The advantage of measuring stationary J - V curves lies in the absence of artifacts associated with capacitance charging/discharging as it occurs in other techniques like linear sweep or cyclic voltammetries (LSV or CV), therefore the obtained results are more reliable. Thus, the J - V curve for a solution of 25 mM of **1a** illustrates that the onset potential (1.375 V vs RHE) is displaced 0.15 V vs the onset of water oxidation without artifacts (Figure 7). In addition, the current increases linearly until reaching a narrow plateau of 52 mA/cm² at 1.75V vs RHE, indicating the limit for efficient amine dehydrogenation. At higher potentials, OER becomes dominant and therefore if we apply these potentials, FE towards **1a** will be reduced.

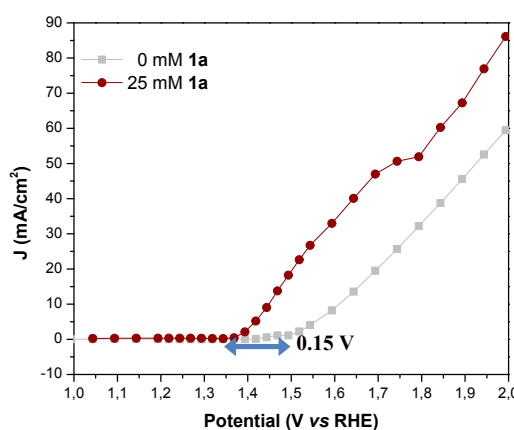
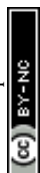


Figure 7. J - V curves obtained during IS measurement of NiNF electrodes in a 0.5M KOH aqueous solution with and without **1a**.

Impedance spectra for samples with and without **1a** is plot in Figure 8. In a first approach, three distinct arcs are evident for each system. The small arc at high frequencies is associated with the electrical contact with the nickel foam electrode. The large, deformed arc at middle frequencies is linked to charge transport, transfer, and accumulation in the NiNF electrode, which is modelled using the transmission line-based equivalent circuit.¹⁹ Finally, the small arc at low frequencies is connected to the diffusion of active species in the solution.

Impedance spectroscopy reveals that the displacement of the arcs along the X-axis and their size are smaller in the presence of **1a** (Figure 8). The X-axis displacement is associated to the series resistance of the sample, R_s , which arises from multiple



contributions, including the NiNF section out of the electrolyte ($R_{S, NiNF}$), the solution bulk resistance ($R_{S, sol}$), and the negligible contributions from contacts and wires, all leading to $R_S \approx R_{S, NiNF} + R_{S, sol}$. In all cases the length of the NiNF outside the solution remains constant. Therefore, we attribute the variance in series resistance among the samples to the increased conductivity of the solution following the addition of **1a**.

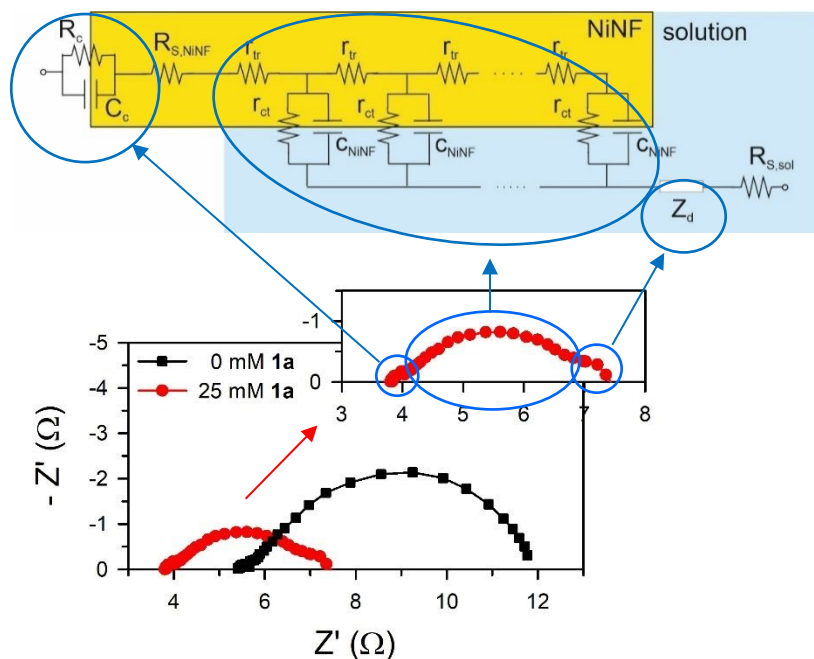


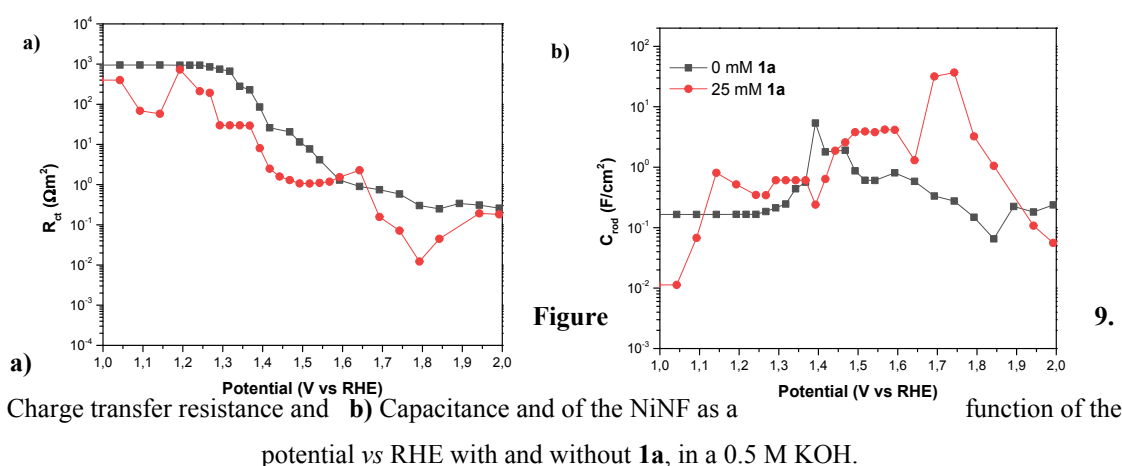
Figure 8. Nyquist plot for the NiNF electrode with and without **1a**, in 0.5 M KOH at 1.5 V vs RHE. Inset shows the IS with 25mM **1a**. The Figure shows how the equivalent circuit used to fit the data (top), is related to the different arcs. The low frequency arc is associated with diffusion, Z_d . The high frequency arc, with the nickel foam electrode contact and the large middle-frequency arc is related to a transmission line that includes the transport resistance in the Ni foam, ($R_{tr} = r_{tr} \cdot L$), the charge transfer resistance from the Ni to the solution, ($R_{ct} = r_{ct}/L$), and the total capacitance of the electrode, ($C_{NiNF} = c_{NiNF} \cdot L$), being L the length of the Ni foam immersed in the solution. The displacement of the arcs from the X-axis origin is given by the series resistance, (R_S).

As Figure 8 shows, the impedance is dominated by the largest arc at intermediate frequencies, associated to the transmission line which is determined by the overall transport resistance of charges in the NiNF (R_{tr}), the charge transfer resistance from the surface of the electrode towards the solution (R_{ct}), and the total contribution to the capacitance of the electrode (C_{NiNF}), which includes contributions from double layer (Helmholtz) capacitance, the capacitance associated to absorbance of **1a** and its



derivatives, and the capacitance associated to the different redox states of Ni. In the case shown in Figure 9a, the variation in size of the intermediate arc when **1a** is added to the solution, is associated with the reduction of R_{ct} .

Understanding the capacitance and charge transfer of the NiNF electrode is crucial for unraveling the mechanisms influencing the device's performance. As can be observed in Figure 9, this capacitance and charge transfer are closely related. In Figure 9b, the NiNF capacitance is depicted as a function of the potential *vs* RHE. In the absence of **1a**, the capacitance of the NiNF electrode increases in the region of 1.35-1.5 V *vs* RHE, corresponding to the $\text{Ni}^{2+}/\text{Ni}^{3+}$ redox peak observed in cyclic voltammetries. The shape of this peak suggests that both Ni-hydrated and dehydrated phases are present.¹⁹ Subsequently, the capacitance decreases, exhibiting another small peak at 1.6 V *vs* RHE, closely aligned with the onset of the OER. This peak has previously been attributed to the $\text{Ni}^{3+}/\text{Ni}^{4+}$ redox transition, with Ni^{4+} identified as the species involved in the OER,¹⁹ matching very well with the drop in R_{ct} below $10 \Omega \cdot \text{cm}^{-2}$ seen in Figure 9a, indicating an acceleration in the kinetics of the process, and the onset of OER shown in Figure 7.



In the presence of **1a**, a broad C_{NiNF} peak is observed between 1.4 and 1.6 V *vs* RHE, which corresponds to the combination of the $\text{Ni}^{2+}/\text{Ni}^{3+}$ redox transition peak and the oxidation peak of **1a**. Notably, this peak aligns well with the onset of the J - V curve in Figure 7 and the drop of R_{ct} below $10 \Omega \cdot \text{cm}^{-2}$, showing the strong correlation between both phenomena. Between 1.65 and 1.8 V *vs* RHE, a significant peak is observed, followed by the dominance of OER in the J - V curve. Two plausible explanations for this peak could be considered: *i*) an oxidation process of intermediates to adiponitrile, or *ii*) the $\text{Ni}^{3+}/\text{Ni}^{4+}$ redox transition. The completion of reactions at 1.55 V *vs* RHE and the



absence of overoxidation products favor the likelihood of the second option. The substantial difference in the height of the $\text{Ni}^{+3}/\text{Ni}^{+4}$ peaks may be attributed to the competition between the oxidation process of **1a** and OER. In the absence of **1a**, once Ni^{+4} is formed, it promptly oxidizes water, resulting in a small charge accumulation in these states. Conversely, with the addition of **1a**, most of the charge transfer is directed toward this species and its intermediates, contributing to the observed high faradaic efficiency. As charge transfer for OER is more challenging, Ni^{+4} may accumulate, leading to higher capacitance. Further R_{ct} decrease is observed in Figure 9a for the same solution.

Another noteworthy observation derived from capacitance measurements is the shift of the two Ni redox peaks towards more positive potentials in the presence of **1a**. This shift is attributed to the interaction of this species with the surface of NiNF electrode. Describing it as a coating of the surface is challenging, as the capacitance of NiNF at potentials below 1.3 V vs RHE in the presence of **1a** is greater than in its absence. Conversely, the adsorption of **1a** could lead to an increase in capacitance, akin to what has been previously observed for hydrogen absorption on Pd-decorated electrodes.²⁶ Finally, at the higher potentials, R_{ct} becomes so small that R_{tr} and R_s dominate J - V curve both for the samples with and without **1a**.

Summarizing the impedance results, the substantial changes in capacitance observed in the NiNF electrode upon the addition of **1a** facilitates to understand the potentials at which Ni and **1a** redox processes occur and even distinguishing the number of oxidation species accumulated in the electrode. The observation of a large accumulation of Ni^{+4} on the electrode with **1a** in solution, together with the shifts in redox peaks observed, suggest the absorption of **1a** species and its derivatives on the electrode surface, that consequently promotes the dehydrogenation reaction. Through resistance analysis, the underlying mechanisms governing the behaviour of J - V curves at all measured potentials are identified. Charge transfer predominates for most potentials, except at higher potentials where limitations due to series resistance control the system's response.

Hydrogenation (reduction) experiments

To complete the dehydrogenation/hydrogenation studies for the utilization of amine/nitrile pair as LOHCs, we explored the reverse process namely, the hydrogenation of nitriles (Figure 10). Several catalysts and different conditions were tested for the hydrogenation of adiponitrile (**2a**) to **1a**, including Pd, Ru and Ni, using molecular hydrogen (H_2) as the hydrogen source (Table S3). The best performance in terms of



conversion, yield and selectivity was achieved with Ni Raney that afforded quantitative yields in short reaction times (6 h).

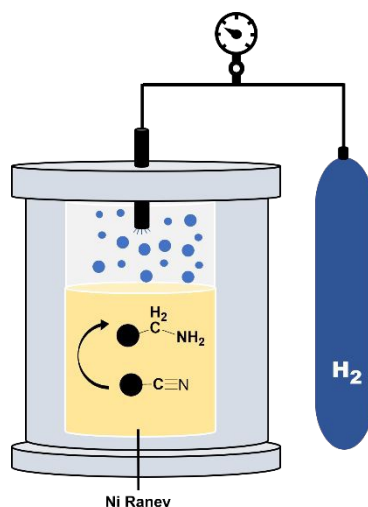


Figure 10. Scheme of high-pressure reactor.

Using this heterogeneous catalyst, among the different products that could be obtained in the hydrogenation of **2a**, 1,6-hexanediamine was obtained in 94% yield, observing very low or null formation of cyclization species and condensation products.

Table 4. Hydrogenation of adiponitrile using Ni Raney as catalyst

Entry	Substrate	Yield (%)
1	1,6-hexanediamine (1a)	94
2	1-amino-5-cyanopentane (i)	0
3	1-amino-6-iminohexane (ii)	0
4	Azepane (iii)	5
5	Condensation products	1

Reaction conditions: adiponitrile (0.15 mmol), iPrOH (1 mL + 100 μ L of 28% aqueous NH_4OH), 20 H_2 bar, 80 $^\circ\text{C}$, 6h. Yields determined by ^1H -NMR spectroscopy and GC/FID.

Conclusions

In this study, we have showcased the effectiveness of Ni electrodes in the selective electrochemical dehydrogenation of both aromatic and aliphatic amines, yielding the corresponding nitriles and molecular hydrogen. Exceptional yields and high faradaic efficiencies were achieved in the dehydrogenation of 1,6-hexanediamine using easily prepared Ni-based electrodes, underscoring the remarkable efficiency of this



electrocatalyst in the reaction. Rigorous impedance analysis has provided valuable insights into the reaction mechanism, elucidating the pivotal role of amine adsorption on the electrode surface in facilitating dehydrogenation. Additionally, the completion of the reaction is contingent upon the diffusion of the amine, highlighting its significance as the decisive step in the process. Our investigations suggest that the electrocatalytic dehydrogenation of primary amines with NiNF electrodes and the catalytic hydrogenation of nitriles by Ni/Raney in aqueous media represents a promising solution for utilizing this pair as liquid organic hydrogen carriers. This reversible pathway offers a safe and environmentally friendly method for storing hydrogen. Furthermore, the mild conditions of this method render it suitable for potential large-scale industrial applications.

Acknowledgements

This study forms part of the Advanced Materials programme and was supported by MCIN with funding from European Union NextGenerationEU (PRTR-C17.I1) and by Generalitat Valenciana under the project MFA/2022/043. The authors want to thank project UJI-B2022-33, funded by University Jaume I and Servicio Central de Instrumentación Científica (SCIC) from Universitat Jaume I. N.G. acknowledges PROMETEO/2020/028, funded by Generalitat Valenciana.

Author Contributions

The manuscript was written through contributions of all authors. All authors have given approval to the final version of the manuscript.

Declaration of Competing Interest

The authors declare that they have no known competing financial interests or personal relationships that could have appeared to influence the work reported in this paper.

Supporting Information

Additional characterization by IS, NMR, GC and SEM.

Author Information

Nihal Guenani, elguenan@uji.es

ORCID: 0000-0003-2346-4951

Jose Solera, jsolera@uji.es

ORCID: 0000-0003-3513-7069

David Carvajal, dcarvaja@uji.es

ORCID: 0000-0003-3723-0371



Andrés Mollar-Cuni, amollar@uji.es

ORCID: 0000-0002-6399-4722

View Article Online
DOI: 10.1039/D4GC01275E

Carmen Mejuto, mejuto@uji.es

ORCID: 0000-0002-4432-5697

Jose A Mata, jmata@uji.es

ORCID: 0000-0001-9310-2783

Francisco Fabregat-Santiago, fabresan@uji.es

ORCID: 0000-0002-7503-1245

Antonio Guerrero, aguerrer@uji.es

ORCID: 0000-0001-8602-1248

Elena Mas-Marzá, emas@uji.es

ORCID: 0000-0002-2308-0635

Institute Twitter username: @inam_uji,

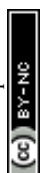
Researcher Twitter username: @jose_mata_uji

References

- (1) Chu, S.; Majumdar, A. Opportunities and Challenges for a Sustainable Energy Future. *Nature*. August 16, 2012, pp 294–303. <https://doi.org/10.1038/nature11475>.
- (2) Preuster, P.; Papp, C.; Wasserscheid, P. Liquid Organic Hydrogen Carriers (LOHCs): Toward a Hydrogen-Free Hydrogen Economy. *Acc Chem Res* 2017, 50 (1), 74–85. <https://doi.org/10.1021/acs.accounts.6b00474>.
- (3) Teichmann, D.; Arlt, W.; Wasserscheid, P.; Freymann, R. A Future Energy Supply Based on Liquid Organic Hydrogen Carriers (LOHC). *Energy and Environmental Science*. August 2011, pp 2767–2773. <https://doi.org/10.1039/c1ee01454d>.
- (4) Crabtree, R. H. Nitrogen-Containing Liquid Organic Hydrogen Carriers: Progress and Prospects. *ACS Sustain Chem Eng* 2017, 5 (6), 4491–4498. <https://doi.org/10.1021/acssuschemeng.7b00983>.
- (5) Crabtree, R. H. Hydrogen Storage in Liquid Organic Heterocycles. *Energy and Environmental Science*. 2008, pp 134–138. <https://doi.org/10.1039/b805644g>.
- (6) Rao, P. C.; Yoon, M. Potential Liquid-Organic Hydrogen Carrier (Lohc) Systems: A Review on Recent Progress. *Energies (Basel)* 2020, 13 (22). <https://doi.org/10.3390/en13226040>.
- (7) Ventura-Espinosa, D.; Carretero-Cerdán, A.; Baya, M.; García, H.; Mata, J. A. Catalytic Dehydrogenative Coupling of Hydrosilanes with Alcohols for the Production of Hydrogen On-Demand: Application of a Silane/Alcohol Pair as a Liquid Organic Hydrogen Carrier. *Chemistry - A European Journal* 2017, 23 (45), 10815–10821. <https://doi.org/10.1002/chem.201700243>.
- (8) Ventura-Espinosa, D.; Sabater, S.; Carretero-Cerdán, A.; Baya, M.; Mata, J. A. High Production of Hydrogen on Demand from Silanes Catalyzed by Iridium Complexes as a Versatile Hydrogen Storage System. *ACS Catal* 2018, 8 (3), 2558–2566. <https://doi.org/10.1021/acscatal.7b04479>.



- (9) Crabtree, R. H. Hydrogen Storage in Liquid Organic Heterocycles. *Energy and Environmental Science*. 2008, pp 134–138. <https://doi.org/10.1039/b805644g>. View Article Online
DOI: 10.1039/D4GC01275E
- (10) Andersson, J.; Grönkvist, S. Large-Scale Storage of Hydrogen. *International Journal of Hydrogen Energy*. Elsevier Ltd May 3, 2019, pp 11901–11919. <https://doi.org/10.1016/j.ijhydene.2019.03.063>.
- (11) Chamoun, R.; Demirci, U. B.; Miele, P. Cyclic Dehydrogenation-(Re)Hydrogenation with Hydrogen-Storage Materials: An Overview. *Energy Technology*. Wiley-VCH Verlag February 1, 2015, pp 100–117. <https://doi.org/10.1002/ente.201402136>.
- (12) Zhu, Q. L.; Xu, Q. Liquid Organic and Inorganic Chemical Hydrides for High-Capacity Hydrogen Storage. *Energy and Environmental Science*. Royal Society of Chemistry February 1, 2015, pp 478–512. <https://doi.org/10.1039/c4ee03690e>.
- (13) Ventura-Espinosa, D.; Marzá-Beltrán, A.; Mata, J. A. Catalytic Hydrogen Production by Ruthenium Complexes from the Conversion of Primary Amines to Nitriles: Potential Application as a Liquid Organic Hydrogen Carrier. *Chemistry - A European Journal* 2016, 22 (49), 17758–17766. <https://doi.org/10.1002/chem.201603423>.
- (14) Cho, J.; Kim, B.; Venkateshalu, S.; Chung, D. Y.; Lee, K.; Choi, S. II. Electrochemically Activatable Liquid Organic Hydrogen Carriers and Their Applications. *J Am Chem Soc* 2023, 145 (31), 16951–16965. <https://doi.org/10.1021/jacs.2c13324>.
- (15) Huang, Y.; Chong, X.; Liu, C.; Liang, Y.; Zhang, B. Boosting Hydrogen Production by Anodic Oxidation of Primary Amines over a NiSe Nanorod Electrode. *Angewandte Chemie - International Edition* 2018, 57 (40), 13163–13166. <https://doi.org/10.1002/anie.201807717>.
- (16) Xiang, M.; Xu, Z.; Wu, Q.; Wang, Y.; Yan, Z. Selective Electrooxidation of Primary Amines over a Ni/Co Metal-Organic Framework Derived Electrode Enabling Effective Hydrogen Production in the Membrane-Free Electrolyzer. *J Power Sources* 2022, 535. <https://doi.org/10.1016/j.jpowsour.2022.231461>.
- (17) Bender, M. T.; Choi, K. S. Electrochemical Dehydrogenation Pathways of Amines to Nitriles on NiOOH. *JACS Au* 2022, 2 (5), 1169–1180. <https://doi.org/10.1021/jacsau.2c00150>.
- (18) Guenani, N.; Barawi, M.; Villar-García, I. J.; Bisquert, J.; De La Peña O'Shea, V. A.; Guerrero, A. Highly Porous Ti-Ni Anodes for Electrochemical Oxidations. *Sustain Energy Fuels* 2020, 4 (8), 4003–4007. <https://doi.org/10.1039/d0se00242a>.
- (19) Arcas, R.; Koshino, Y.; Mas-Marzá, E.; Tsuji, R.; Masutani, H.; Miura-Fujiwara, E.; Haruyama, Y.; Nakashima, S.; Ito, S.; Fabregat-Santiago, F. Pencil Graphite Rods Decorated with Nickel and Nickel-Iron as Low-Cost Oxygen Evolution Reaction Electrodes. *Sustain Energy Fuels* 2021, 5 (15), 3929–3938. <https://doi.org/10.1039/d1se00351h>.
- (20) Lu, G. P.; Li, X.; Zhong, L.; Li, S.; Chen, F. Ru@UiO-66(Ce) Catalyzed Acceptorless Dehydrogenation of Primary Amines to Nitriles: The Roles of Lewis Acid-Base Pairs in the Reaction. *Green Chemistry* 2019, 21 (19), 5386–5393. <https://doi.org/10.1039/c9gc02181g>.



- (21) Tseng, K. N. T.; Rizzi, A. M.; Szymczak, N. K. Oxidant-Free Conversion of Primary Amines to Nitriles. *J Am Chem Soc* 2013, *135* (44), 16352–16355. <https://doi.org/10.1021/ja409223a>. View Article Online
DOI: 10.1039/D4GC01275E
- (22) Dutta, I.; Yadav, S.; Sarbajna, A.; De, S.; Hölscher, M.; Leitner, W.; Bera, J. K. Double Dehydrogenation of Primary Amines to Nitriles by a Ruthenium Complex Featuring Pyrazole Functionality. *J Am Chem Soc* 2018, *140* (28), 8662–8666. <https://doi.org/10.1021/jacs.8b05009>.
- (23) Achard, T.; Egly, J.; Sigrist, M.; Maisse-François, A.; Bellemin-Lapponnaz, S. Easy Ruthenium-Catalysed Oxidation of Primary Amines to Nitriles under Oxidant-Free Conditions. *Chemistry - A European Journal* 2019, *25* (58), 13271–13274. <https://doi.org/10.1002/chem.201902557>.
- (24) Carvajal, D.; Arcas, R.; Gouda, L.; Fabregat-Santiago, F.; Mas-Marzá, E. Electrochemical Valorization of HMF Using Ni/Graphite Electrodes. *Mater Chem Phys* 2024, *311*. <https://doi.org/10.1016/j.matchemphys.2023.128510>.
- (25) Gouda, L.; Sévery, L.; Moehl, T.; Mas-Marzá, E.; Adams, P.; Fabregat-Santiago, F.; Tilley, S. D. Tuning the Selectivity of Biomass Oxidation over Oxygen Evolution on NiO-OH Electrodes. *Green Chemistry* 2021, *23* (20), 8061–8068. <https://doi.org/10.1039/d1gc02031e>.
- (26) Carvajal, D.; Arcas, R.; Mesa, C. A.; Giménez, S.; Fabregat-Santiago, F.; Mas-Marzá, E. Role of Pd in the Electrochemical Hydrogenation of Nitrobenzene Using CuPd Electrodes. *Adv Sustain Syst* 2022, *6* (4). <https://doi.org/10.1002/adsu.202100367>.

